Convectively Coupled Equatorial Waves: A New Methodology for Identifying Wave Structures in Observational Data

Gui-Ying Yang, Brian Hoskins, and Julia Slingo

Centre for Global Atmospheric Modelling, Department of Meteorology, University of Reading, Reading, United Kingdom

ABSTRACT

Convectively coupled equatorial waves are fundamental components of the interaction between the physics and dynamics of the tropical atmosphere. A new methodology, which isolates individual equatorial wave modes, has been developed and applied to observational data. The methodology assumes that the horizontal structures given by equatorial wave theory can be used to project upper- and lower-tropospheric data onto equatorial wave modes. The dynamical fields are first separated into eastward- and westward-moving components with a specified domain of frequency–zonal wavenumber. Each of the components for each field is then projected onto the different equatorial modes using the y structures of these modes given by the theory. The latitudinal scale y_o of the modes is predetermined by data to fit the equatorial trapping in a suitable latitude belt $y = \pm Y$. The extent to which the different dynamical fields are consistent with one another in their depiction of each equatorial wave structure determines the confidence in the reality of that structure. Comparison of the analyzed modes with the eastward- and westward-moving components in the convection field enables the identification of the dynamical structure and nature of convectively coupled equatorial waves.

In a case study, the methodology is applied to two independent data sources, ECMWF Reanalysis and satellite-observed window brightness temperature (T_b) data for the summer of 1992. Various convectively coupled equatorial Kelvin, mixed Rossby–gravity, and Rossby waves have been detected. The results indicate a robust consistency between the two independent data sources. Different vertical structures for different wave modes and a significant Doppler shifting effect of the background zonal winds on wave structures are found and discussed.

It is found that in addition to low-level convergence, anomalous fluxes induced by strong equatorial zonal winds associated with equatorial waves are important for inducing equatorial convection. There is evidence that equatorial convection associated with Rossby waves leads to a change in structure involving a horizontal structure similar to that of a Kelvin wave moving westward with it. The vertical structure may also be radically changed.

The analysis method should make a very powerful diagnostic tool for investigating convectively coupled equatorial waves and the interaction of equatorial dynamics and physics in the real atmosphere. The results from application of the analysis method for a reanalysis dataset should provide a benchmark against which model studies can be compared.

1. Introduction

The complete picture of the tropical atmosphere involves the interaction of convection and other physical processes with each other and with the dynamics, both locally and globally. Equatorial waves have been used to explain some fundamental phenomena of the tropical climate, such as the Walker circulation (e.g., Gill 1980), atmospheric teleconnection patterns (e.g., Lim and Chang 1983), the Madden–Julian oscillation (MJO; e.g., Lau and Peng 1987), and the El Niño–Southern Oscillation (ENSO; e.g., Lau 1981), as well as the forcing of the equatorial quasi-biennial oscillation (QBO) and semiannual oscillation (SAO; e.g., Lindzen and Holton

1968). During the Tropical Ocean Global Atmosphere Coupled Ocean–Atmosphere Response Experiment (TOGA COARE), for example, a substantial fraction of the large-scale variability in convection at timescales less than 30 days has been attributed to equatorially trapped modes (Redelsperger et al. 1998). Hence, convectively coupled equatorial waves are a key part of the tropical climate system and as such, it is essential that global circulation models (GCM) are able to represent them adequately.

However, at present there is limited knowledge of these waves, their structures and how well they are treated in state-of-the-art models. A key question here is the relationship between the dynamical structure and the convection. This is of practical importance and a faithful representation of it is needed for predictions on all timescales. The research described in this paper is intended to provide a basic framework that will enable the un-

Corresponding author address: Gui-Ying Yang, Dept. of Meteorology, University of Reading, Earley Gate, Reading RG6 6BB, United Kingdom.
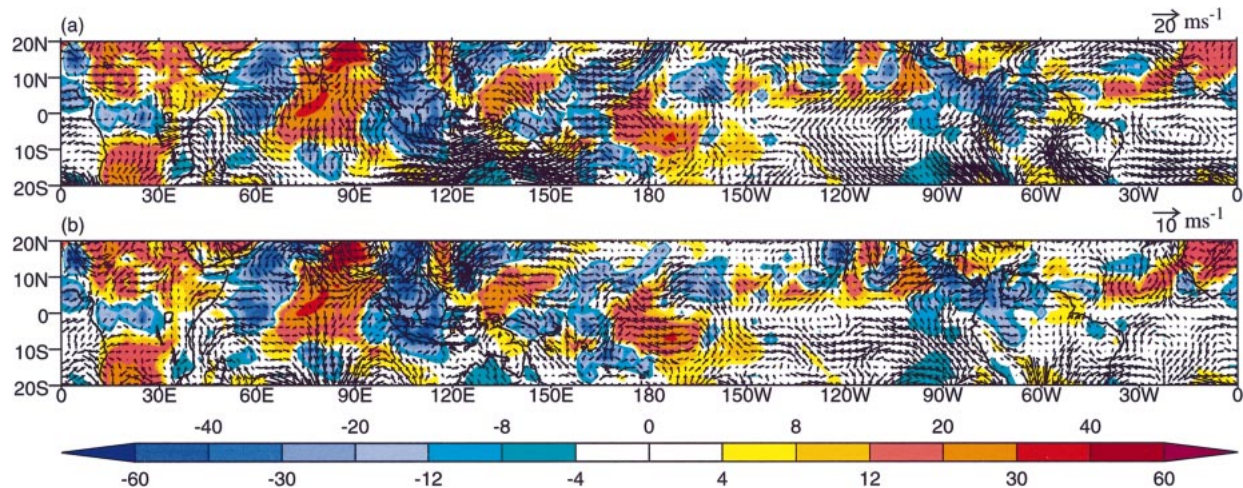E-mail: swsyangg@met.reading.ac.uk

FIG. 1. An example of horizontal winds from the ERA daily data at 1200 UTC 13 Jul 1992 for (a) 200 hPa and (b) 850 hPa. Superimposed colors show the CLAUS brightness temperature T_b for the same day. Units are m s^{-1} for wind and K for T_b.

derstanding of convectively coupled waves and help the answering of such questions.

Tropical convection contains variability on a variety of space and timescales, ranging from the individual clouds, through the cloud clusters associated with synoptic-scale disturbances, to the super clusters or ensembles of clusters. Synoptic activity in the Tropics is often associated with disturbances, which can be related to the preferred equatorially trapped modes of the atmospheric circulation based on shallow water theory (e.g., Takayabu 1994a,b; Wheeler and Kiladis 1999; Wheeler et al. 2000). Various modes (Kelvin, mixed Rossby–gravity, equatorial Rossby, and gravity waves) can be detected, in many cases related to the active phase of the MJO (Madden and Julian 1972), thus demonstrating the important interaction between synoptic and intraseasonal timescales.

It is clear from various studies (e.g., Takayabu 1994a,b) that analysis of high-resolution satellite data can provide information on equatorial waves and the diurnal cycle that should be essential validation for GCMs. An extended record of global cloud variability on a wide range of spatial and temporal scales has been provided by the Cloud Archive User Service (CLAUS), a European Union part-funded initiative to establish a long-term, continuous archive of global brightness temperature (T_b) data, spanning the period 1984 to 1999. The source data for CLAUS are the intermediate-level (B3) products generated by the International Satellite Cloud Climatology Project (ISCCP) from meteorological and other satellite observations from 1984 onward. The data for CLAUS are generated by resampling the window brightness temperatures from the B3 data on to a global grid at a resolution of 0.5° and 3 h. More detailed description of the algorithm for generating the CLAUS dataset and of the dataset itself can be found in Hodges et al. (2000) and Yang and Slingo (2001).

In addition to the CLAUS dataset, the European Cen-

tre for Medium-Range Weather Forecasts (ECMWF) Reanalysis (ERA-15) is used. ERA has been performed at relatively high resolution (spectral truncation at 106 wavenumbers, equivalent to grid resolution of ~1.125°) and is contemporary with the CLAUS data. The combination of the ERA and CLAUS data represents a unique opportunity to diagnose the relationship between the dynamical structure and convective organization of equatorial waves.

To identify and describe the structure of convectively coupled equatorially trapped modes in observational data, an essential step is to separate the various equatorial wave modes. Figure 1 gives an example of the convection field, as described by the window brightness temperature, and ERA wind fields in the upper and lower troposphere on 13 July 1992. The monthly mean has been removed from each field to highlight the variability on timescales of less than 1 month. It can be seen that there are rich features in the convection and dynamical fields. Some possible signatures of equatorial waves can be seen, for example, the strong cross-equatorial meridional wind in the upper troposphere around the eastern Pacific and Central America, and in the lower troposphere over Central America, together with convection that is asymmetric about the equator, suggestive of a mixed Rossby–gravity wave. However, it is difficult to identify, uniquely, individual wave structures and their associated convection.

Equatorial waves, coupled with convection, have been studied for several decades since satellite data became available (e.g., Gruber 1974; Zangvil 1975; Zangvil and Yanai 1981; Hendon and Liebmann 1991; Takayabu 1994a,b; Dunkerton and Baldwin 1995; Magaña and Yanai 1995; Wheeler and Kiladis 1999; Wheeler et al. 2000). Most of these studies used spectral analysis of the convection and dynamical fields to provide evidence of equatorial waves. Various methods, such as space–time cross-spectral analysis, linear regression,

and lag correlation, have been used to investigate the relationship between convection and the dynamical fields. Takayabu (1994a,b) used space–time spectral analysis and theoretical equatorial wave dispersion curves to isolate various equatorial wave modes. Wheeler and Kiladis (1999), based on space–time spectral analysis of satellite-observed outgoing longwave radiation (OLR), designed a selective filtering of OLR to isolate the convective variations contributing to spectral peaks, which coincide with the equatorial wave dispersion curves for various equivalent depths. Their study suggested that a portion of the space–time variability of deep tropical cloudiness inferred from OLR could be described quite well in terms of equatorially trapped wave modes from shallow water theory. Their following companion paper (Wheeler et al. 2000) used linear regression between selectively filtered OLR data and various dynamical fields to obtain dynamical structures of the waves. These dynamical structures showed an impressive agreement with those obtained from equatorial wave theory.

When the CLAUS data became available, we initially used space–time spectral analysis (Hayashi 1982) and a similar technique of selective filtering based on theoretical dispersion relations (Wheeler and Kiladis 1999) to examine the convectively coupled equatorial waves during the summer of 1992. In agreement with Wheeler and Kiladis (1999), analysis of the T_b data (not shown) demonstrated that tropical convection is organized on preferred space and timescales, which coincide approximately with those of theoretical equatorial waves. However, in the real atmosphere the complicated space–time dependence of the ambient state can be expected to lead to Doppler shifting and distortion of the theoretical dispersion curves, and to variations in the vertical heating profile and hence the equivalent depth (h). Consequently, different equatorial modes may not, in reality, be well separated in their frequency and zonal wavenumber domain. Also, convectively coupled modes might be expected to behave rather differently from dry waves, and it is unclear how much of the shallow water theory of equatorial waves can be carried over to the real world. It is evident, therefore, that a new, less constraining methodology for objectively separating equatorial wave structures would be very beneficial and this is the stimulus for this research.

The main aim of the whole study is to develop a new methodology for isolating various equatorial waves, to develop further our understanding of the physics and dynamics of the tropical atmosphere in the context of convectively coupled equatorial waves, and to use that understanding to evaluate the performance of climate and weather forecasting models. This paper describes the first stage of that study, that is, the development of the methodology and demonstration of its utility in a case study of equatorial waves in 8 days of observational data. In a companion paper we will apply the methodology to the entire season to provide statistics on observed equatorial wave characteristics. It is hoped that this will serve as a test bed for weather and climate prediction models.

The outline of this paper is as follows. The theoretical background for equatorial waves will be briefly introduced in the next section. The details of the methodology will be described in section 3. In section 4, the methodology is applied to the ERA and CLAUS data and examples of westward- and eastward-moving equatorial wave activities isolated from the observational data are shown. Conclusions and discussion will appear in section 5.

2. Equatorial wave theory

Following Matsuno (1966), Gill (1980, 1982), and many others, equatorially trapped waves are obtained as solutions to the adiabatic, frictionless equations of motion on an equatorial β plane linearized about a state of rest. The representation of the two horizontal-velocity (u, v) and geopotential-height (ϕ) fields are of the form

$$\{u', v', \phi\}$$
$$= A(z)\{u(y), v(y), \phi(y)\} \exp[i(kx - \omega t)], \quad (2.1)$$

where k is the zonal wavenumber and ω is the frequency. The common, separated vertical structure function $A(z)$ is a solution of an equation that can also satisfy relevant surface and upper boundary conditions; this is possible only for discrete values of the separation constant, c. The first internal mode has one zero in A in the troposphere and extrema of opposite sign near the tropopause and the surface. A typical value for c for this mode is in the range of 25–50 m s^{-1}. Higher vertical modes with additional zeros (nodes) in A correspond to successively smaller values of c.

The horizontal and temporal behavior of $\{u', v', \phi'\}$ satisfies the linearized shallow water equations with gravity wave speed c, the separation constant from the vertical structure equation. However, the equatorial wave solutions are most easily formulated in terms of new variables, q, r, and v (Gill 1980), where

$$q = (g/c)\phi + u \quad \text{and} \quad r = (g/c)\phi - u. \quad (2.2)$$

The dispersion relation for the waves is found to be

$$\omega = kc, \quad \text{for the Kelvin wave} \quad \text{and} \quad (2.3a)$$

$$\frac{\omega^2}{c^2} - k^2 - \frac{\beta k}{\omega} = (2n + 1)\frac{\beta}{c},$$
$$\text{for } n = 0, 1, 2, \ldots, \quad (2.3b)$$

where n is the meridional wavenumber and β is $\partial f / \partial y$. Solutions of this dispersion relation with $c = 20$ m s^{-1} are summarized in Fig. 2a.

The Kelvin wave (K) satisfies Eq. (2.3b) with $n = -1$ and is often referred to in this manner. For $n \geq 1$, Eq. (2.3b) has three roots. The first, the Rossby wave (Rn), corresponds to small westward phase speed; the other two roots correspond to fast-moving westward and
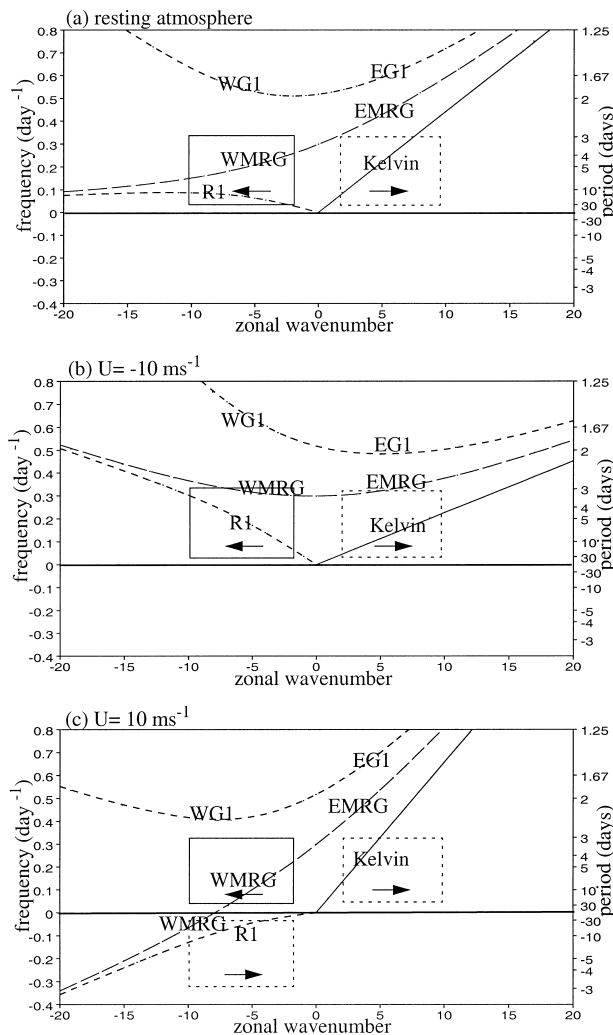
FIG. 2. Dispersion curves of equatorial waves for (a) a resting atmosphere, (b) -10 m s^{-1}, and (c) 10 m s^{-1} basic states. The boxes in each of the panels indicate the wavenumber and frequency bands that will be investigated in this paper, the dashed boxes are for eastward-moving waves and the solid boxes are for westward.

eastward gravity waves (WGn and EGn, respectively). For $n = 0$ there is one root ($\omega = -kc$), which is an artifact of the elimination procedure, and two further roots corresponding to westward- and eastward-moving components of the so-called mixed Rossby–gravity wave (WMRG and EMRG). At high wavenumbers, WMRG resembles a Rossby wave and EMRG, a gravity wave. In Fig. 2, the westward-moving waves are shown for negative k and positive ω, this being a reflection of the situation in the positive k, negative ω quarter plane.

The meridional (y) structure of the waves is given in terms of parabolic cylinder functions (D), which take the form

$$D_r(y/y_o) = \exp[-(y/2y_o)^2]P_r(y/y_o), \qquad (2.4)$$

where P_r is a polynomial of degree r, and y_o is the trapping scale given by

TABLE 1. The structures of theoretical equatorial wave solutions for the Kelvin (K), the WMRG, EMRG, the R1, the WG1, EG1, and the R2 waves. Parameter n is the meridional mode number, D_n is a parabolic cylinder function as in Eq. (2.4), v is meridional wind, and q and r are as in Eq. (2.2).

Value of n	Westward	Eastward	q	v	r
-1		K	$q_0 D_0$	0	0
0	WMRG	EMRG	$q_1 D_1$	$v_0 D_0$	0
1	R1, WG1	EG1	$q_2 D_2$	$v_1 D_1$	$r_0 D_0$
$n > 1$	Rn, WGn	EGn	$q_{n+1} D_{n+1}$	$v_n D_n$	$r_{n-1} D_{n-1}$

$$y_o = (c/2\beta)^{1/2}. \qquad (2.5)$$

The structures of the waves are summarized in Table 1. The coefficients of the structures for q, v, and r are related through

$$q_{n+1} = \frac{\sqrt{2\beta c}}{i(ck - \omega)} v_n \quad \text{and} \qquad (2.6a)$$

$$r_{n-1} = \frac{n\sqrt{2\beta c}}{i(ck + \omega)} v_n. \qquad (2.6b)$$

Some aspects of the structure of the gravest horizontal modes are illustrated in Fig. 3. Westward-moving waves are shown in the left column, and eastward-moving waves in the right column. The vectors indicate the lower-tropospheric wind fields. (Note that, for the first internal mode, the upper-tropospheric wind fields would be in the opposite direction.) The colors indicate the lower-tropospheric divergence field, and for the first internal mode, also show the midtropospheric vertical motion. The Kelvin wave is composed of purely zonal motion and has obvious equatorial convergence. The mixed Rossby–gravity wave has a maximum in meridional wind on the equator. Off the equator for WMRG, this meridional wind is part of a horizontal, predominantly rotational, circulation, whereas for EMRG the off-equatorial zonal wind enhances the convergence and divergence. In each case, the divergence field is in the same sense as implied by the convergence of the meridional wind, but for a given meridional wind strength it is much stronger for the EMRG. The R1 wave has rotational flow centered off the equator with convergence in the region of poleward-moving air, as required by vorticity (Sverdrup) balance. For the R2 wave, the main rotational flow and divergence extrema are further from the equator and have symmetry across the equator which is opposite to that for R1. The westward- and eastward-moving inertio-gravity waves, WG1 and EG1, are dominated by their divergent meridional components with opposite senses for the zonal wind in the two waves.

If the low-level convergence and upper-level divergence in the first internal mode, with associated midtropospheric ascent, provide the organization for convection, then we would expect this convection to occur in the blue–green shaded regions in Fig. 3. However, for convectively coupled waves, wind-dependent sur-
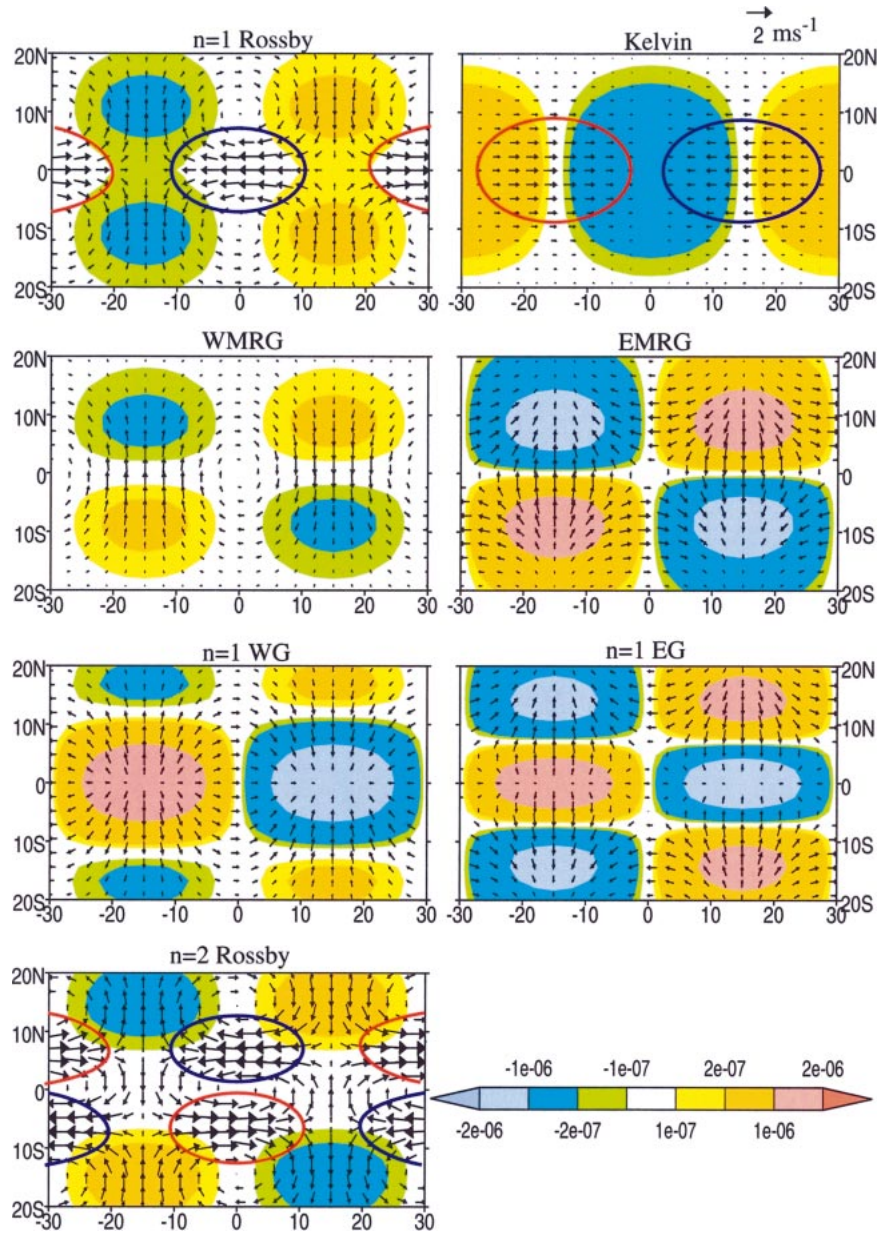
FIG. 3. Dimensional horizontal wind (vector) and divergence (color) solutions of theoretical equatorially trapped Kelvin wave with zonal wind $u_o D_o(y/y_o) \exp[i(kx - \omega t)]$ and other $n = 0 \sim 2$ waves with meridional wind $v_n D_n(y/y_o) \exp[i(kx - \omega t)]$, where n is the meridional mode number, $u_o = v_n = 1$ m s^{-1}, D_n is a parabolic cylinder function, the trapping scale $y_o = 6°$ and zonal wavenumber $k = 6$. The y_o and k are chosen based on an analysis of observational data in section 3 for the convenience of comparison. The waves shown are the Kelvin, the WMRG, the EMRG, the R1, the WG1, the EG1, and the R2 waves. Units are m s^{-1} for wind and s^{-1} for divergence. Color circles for Kelvin and Rossby waves indicate the possible convection region induced by wind-dependent surface energy fluxes.

face fluxes of moist entropy may play an important organizational role for convection. Emanuel (1987) and Neelin et al. (1987) proposed a mechanism of wind-induced surface heat exchange (WISHE) or evaporation–wind feedback, as being crucial in driving MJO-related convection. In situ observational studies and global model analyses have shown that in the western

Pacific region positive anomalies of atmospheric deep convection associated with the MJO tend to occur in regimes of enhanced surface westerly flow, rather than in phase with the low-level convergence (e.g., Zhang 1996; Zhang and McPhaden 2000; Hendon and Salby 1994). These studies concentrated on the intraseasonal timescale and very low zonal wavenumber, and the role
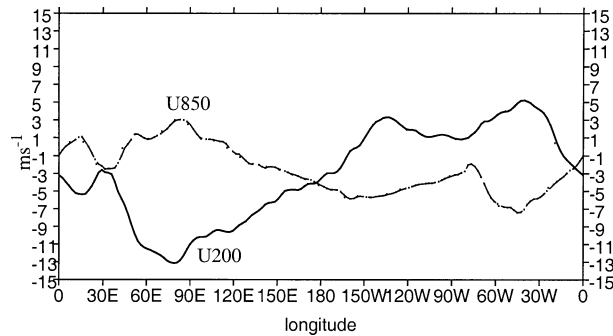
FIG. 4. ERA zonal mean zonal winds at 200 and 850 hPa averaged over 10°N–10°S for 1992 summer (May–Oct).

of the wind-dependent surface fluxes on shorter time- and smaller space scales of convection is not clear but may be important. It is suggested, therefore, that convection associated with equatorial waves may, in some cases, occur where there are anomalous zonal winds, as well as in the expected regions of low-level convergence. Remembering that in the real world, the warmest SSTs occur in the near-equatorial region and hence predispose the atmosphere to convection, it is here that zonal wind anomalies associated with equatorial waves may make the most significant contribution to the wind-induced surface energy fluxes and hence affect the convection.

Regions where wind-induced surface energy flux extrema and hence equatorial convection are likely to occur in the Kelvin and R1 waves, and possibly also the R2 wave, are shown as the blue and red ovals in Fig. 3. Whether the convection would coincide with the blue or red oval would depend on the sign and magnitude of the background zonal wind. As discussed by Wang (1988), Hendon and Salby (1994), and more recently Moscowitz and Bretherton (2000), frictional convergence may also be important for organizing equatorial convection. In this case the convection would occur in the region of near-surface easterlies (the blue ovals) and would be suppressed in the westerlies (the red ovals). It is possible that the heating associated with the equatorial convection induced by the wind-induced fluxes or frictional convergence may alter the theoretical structures of the Kelvin and Rossby waves. Anticipating the results to be shown later, for the Kelvin wave, this could be just a modification of the dry structure. However, for the Rossby waves, the associated equatorial convection could lead to a radical change in structure and behavior.

In the real atmosphere, many of the approximations made in equatorial wave theory may be expected to break down. For example, the ambient flow in the Tropics is not, in general, close to a state of rest; physical processes such as surface friction and convection are clearly important; and nonlinearity could also be important. Considering, first, the ambient flow, Fig. 4 shows as an example, the seasonal mean zonal wind at 200 and 850 hPa, averaged over 10°N–10°S for the sum-

mer of 1992 (May–October). In general, there are upper-tropospheric westerlies in the Western Hemisphere (0°–180°W) and stronger easterlies in the Eastern Hemisphere (0°–180°E), and the lower-tropospheric winds are weaker than those at the upper troposphere and tend to have an opposite sign to those of the upper level. There is also considerable temporal variability in the magnitude and direction of the wind, with strengths exceeding 20 m s^{-1} in the upper troposphere and 10 m s^{-1} in the lower troposphere, in some instances. Such variations in the ambient flow are likely to have a significant impact on the phase speed and structure of equatorial waves.

For any nonzero basic state, the separation of variables used in the equatorial wave analysis is not strictly possible, although, as in Hoskins and Yang (2000), the effects of Doppler shifting can be suggested by replacing ω by $(\omega - ku)$ in the dispersion relations Eq. (2.3). The results for basic zonal winds of ± 10 m s^{-1} are shown in Figs. 2b and 2c, respectively. The boxes shown in Fig. 2 indicate the range of frequencies (3–30 days) and spatial wavenumbers (2–10) used in this study. Note that, for a resting atmosphere (Fig. 2a) only the Kelvin wave exists in the box for eastward-moving waves. However, an easterly basic state (Fig. 2b) reduces the frequency of eastward-moving waves so that the eastward box also includes low-wavenumber EMRGs, demonstrating the difficulty in uniquely separating individual wave modes using simple space–time filtering. In addition, Fig. 2c shows that a westerly ambient flow advects the westward-moving waves to such an extent that R1 and high-wavenumber WMRG waves are found in the lower left quadrant of negative k and ω (eastward-propagating waves). Whereas the westward box includes R1 and WMRG waves for a resting atmosphere (Fig. 2a) and for an easterly basic state but with increased frequency (Fig. 2b), only low-wavenumber WMRG are found in this box when the ambient flow is westerly (Fig. 2c).

How Doppler shifting will affect equatorial waves will also depend on whether the wave senses the lower- or upper-tropospheric flow or even an average flow. The vertical structure of the ambient flow around the Tropics has already been noted in Fig. 4 and the reversal in sign of the zonal flow between the upper and lower troposphere may suggest that the effects of Doppler shifting may inhibit vertical coupling of the waves. As summarized in Table 2, the zero basic-state dispersion diagram suggests that, in the wavenumber–frequency box under consideration, the westward-moving waves would be the WMRG and Rn, and the eastward-moving waves K and perhaps long EMRG. If there is an element of Doppler shifting, then in the ambient westerlies at low levels in the Eastern Hemisphere and at upper levels in the Western Hemisphere, Rn and short WMRG could be shifted from westward to eastward propagating. In the same region, long EMRG become less likely to be found in the eastward-propagation box. In the regions

TABLE 2. Westward- and eastward-moving equatorial waves in the Eastern (EH) and Western (WH) Hemispheres and the upper and lower tropospheres. The first column shows the expectation from basic theory for zonal wavenumbers 2–10 and periods 3–30 days. The second pair of columns give possible changes suggested by notions of Doppler shifting with the winds at the level. The third pair of columns show the convectively coupled waves actually identified. For the westward-moving waves, the order of the rows is WMRG, Rn, and WG1, and for the eastward, K, EMRG, WMRG, Rn, and EG1. In the basic theory column, "?" means that the wave is on the edge of the wavenumber-frequency box. In the Doppler changes columns, "more" and "less" refer to more or less likely to occur, and "??" means that the wave moves closer to the box but does not occur inside for reasonable wind speeds. In the observed columns, waves are also marked in the dateline (DL) region if they occur there and not in one of the hemispheres. The square bracket means that the sign is often the same as that in the lower troposphere, as opposed to a first baroclinic mode structure. Basic theory suggests that the Kelvin wave may be linked to near-equatorial convective but that the others will have associated off-equatorial convection. Not included in the table is a lower-tropospheric eastward-moving R1 wave with associated equatorial convection only.

Basic	Possible Doppler changes		Observed in 2 weeks		
	EH	WH	EH	DL	WH
WESTWARD					
Upper					
WMRG		WMRG less	WMRG		WMRG
Rn		Rn less	Rn		[R1], R2
		WG1 ??			
Lower					
WMRG	WMRG less			WMRG	WMRG
Rn	Rn less		Rn		Rn
	WG1 ??				
EASTWARD					
Upper					
K			K	K	
EMRG?	EMRG more	EMRG less	EMRG		
		WMRG more			WMRG
		Rn more	Rn		Rn
	EG1??		EG1		
Lower					
K			K	K	
EMRG?	EMRG less	EMRG more			
	WMRG more				
	Rn more		R2		R2
		EG1 ??			

of ambient easterlies the eastward-moving EMRG may be more prevalent. Although they are not shifted into the box for the winds shown, EG1 gets closer for ambient easterly winds and WG1 for westerlies. The possible Doppler shift changes are also summarized in Table 2.

The waves actually found in July 1992 using the methodology described in the next section are also shown in Table 2 and will be discussed in section 4. As stated above, the observed waves can be expected to differ from those given by basic linear theory for a variety of reasons and not just because of advection by the ambient flow.

3. Development of the methodology

a. Overview

As noted earlier, the approximations underlying equatorial wave theory may not be applicable when looking for such waves in the real atmosphere, especially those coupled with deep convection. However, given the results of earlier studies by, for example, Wheeler and Kiladis (1999), which demonstrated the qualitative suc-cess of applying equatorial wave theory to real data, we do not wish to reject the theory completely. In this study we will impose a minimum from the details of the theory and see what structure emerges from the data. The first operation we will perform is a spectral analysis sepa-rating brightness temperature and dynamical fields into eastward- and westward-moving components, and retaining a band of wavenumbers and frequencies. Then we will use T_b variance as a guide for specifying the bounds $\pm Y$ for the tropical strip in which the analysis will be performed. Outside this strip the variation in all the fields will be set to zero.

Parabolic cylinder functions form a complete set of functions and we may represent the basic dynamical fields at any level of the atmosphere in terms of a se-verely truncated series of them. The basic trapping scale y_o for the functions will be determined by the criterion that the truncated series best fit the complete meridional wind field. There will be no assumption that y_o is related by (2.5) to a speed c that is itself determined from a vertical structure.

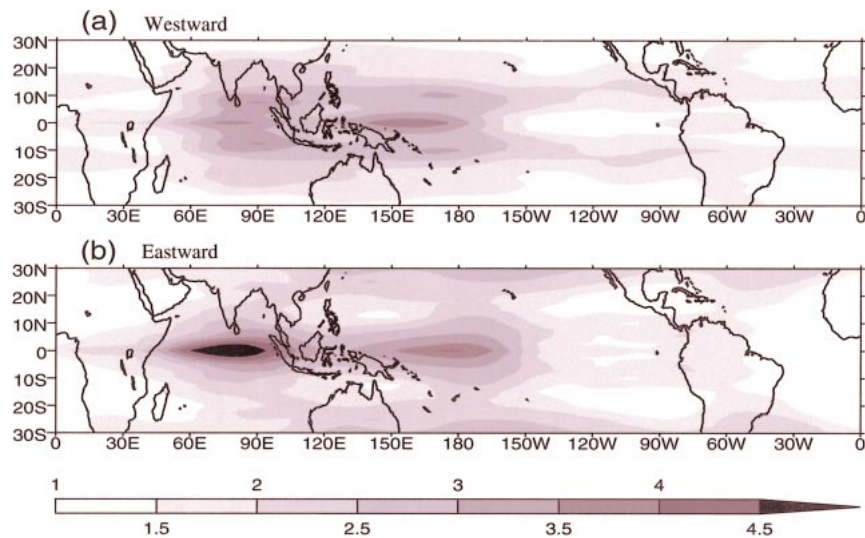In equatorial wave theory, in addition to meridional wind v, the basic dynamical fields that are represented

FIG. 5. Standard deviation of the symmetric component of the brightness temperature T_b in 1992 summer for (a) westward-moving ($k = -2 \sim -10$) and (b) eastward-moving ($k = 2 \sim 10$) components with a period of $3 \sim 30$ days. Unit is K.

by parabolic cylinder functions are $q = \alpha\phi + u$ and $r = \alpha\phi - u$, where $\alpha = g/(2\beta y_o^2)$. For specified y_o, the fitting of u and ϕ by truncated series is independent of the choice of α. However, if we assume that the Kelvin wave is represented by $q_o D_o$ and has zero r, then the condition $\alpha = g/(2\beta y_o^2)$ is necessary for its zonal wind field to be in geostrophic balance. This value for α will be used here, but again not assuming any relationship to a speed c [although according to Eq. (2.5) $\alpha = g/(2\beta y_o^2) = g/c$]. In section 4a, a brief discussion of alternative choices will be given.

It will not be assumed here that the coefficients of v, q, and r are related by (2.6) for some c and ω. Instead, v, q, and r will be analyzed separately. The components of the truncated expansions that, according to equatorial wave theory and summarized in Table 1, would correspond to particular waves are then considered together. For example for the westward-moving features we consider the fields

$$u = \frac{1}{2}(q_2 D_2 - r_0 D_0), \qquad v = v_1 D_1,$$

$$\phi = \frac{1}{2\alpha}(q_2 D_2 + r_0 D_0)$$

as potentially describing a collection of R1 and WG1 waves present on that day. Given that in same region the u and v fields combine and are consistent with the ϕ field then we consider that we may describe a wave as being present. Coherent development and movement of the feature over consecutive analysis periods further supports this interpretation.

We will not assume that there is a particular vertical structure, but instead a separate analysis will be per-

formed in the upper and lower troposphere. If analyses at different levels produce similar waves with a consistent phase relationship we consider that they may describe a 3D structure, developing and moving. If the component of the T_b moving in the same direction shows a feature that has a consistent spatial relationship with the dynamical wave then we consider that we have identified a convectively coupled wave.

b. Application

The space–time spectral analysis, similar to that of Hayashi (1982), is used to separate eastward- and westward-moving waves. The eastward/westward data are then spatially and temporally filtered using fast Fourier transforms (FFT) to retain only frequencies of 3 to 30 days and zonal wavenumbers 2 to 10.[1] The chosen domain contains most of the low-frequency equatorial waves, which are relevant to synoptic and intraseasonal variability in the Tropics. This space–time filtering is applied to the CLAUS T_b and the ERA 200- and 850-hPa u, v, and ϕ fields for 1992 summer (May–October).

To determine the bounds $\pm Y$ of the tropical strip, the T_b coefficients are further decomposed into those symmetric and antisymmetric about the equator.[2] Standard deviations are then calculated for both westward- and eastward-moving components. As an example, Fig. 5

---

[1] Wavenumber 1 is not included in the analysis because of problems with the ERA data. We found an unrealistic level of power at all westward frequencies, particularly in lower-tropospheric geopotential. The reasons for this are not understood.

[2] This equatorial symmetry decomposition of T_b is not used below when looking for convectively coupled aspects of equatorial waves.

shows the eastward and westward components symmetric about the equator. Large variations associated with westward-moving waves appear over a latitude belt that varies from about ±23° over the Indian Ocean/western Pacific to about ±17° over the eastern Pacific (Fig. 5a). In addition to large variations over the tropical region, the eastward-moving waves also show significant activity poleward of 25°, associated with eastward-moving, extratropical Rossby waves (Fig. 5b). Between these two regions, a minimum in activity is seen at about 20°, which separates the activity of equatorial waves from that of extratropical Rossby waves. The corresponding plots for the components antisymmetric about the equator (not shown) give similar results. This suggests that equatorial convectively coupled waves are found primarily between 20°N and 20°S, and therefore it is reasonable to set $Y = 20°$ to calculate the best fit for y_o.

The best fit y_o is chosen in such a way that minimizes the meridional wind analysis errors in the tropical strip. The time-mean analysis error E is defined as follows:

$$E_N(x_i, y_j, y_o)$$

$$= \frac{\sum_k \left[\tilde{v}(x_i, y_j, t_k) - \sum_{n=0}^{N} \tilde{v}_n(x_i, t_k) D_n\left(\frac{y_j}{y_o}\right) \right]^2}{\sum_k [\tilde{v}(x_i, y_j, t_k) - \overline{v}(x_i, y_j)]^2}, \quad (3.1)$$

where (x_i, y_j, t_k) is a space–time grid point of the data, and $\tilde{v}$ represents the variable v filtered to give its eastward-/westward-moving component in the specified frequency–zonal wavenumber domain $\{\omega, k\}$; $\tilde{v}_n$ is the coefficient of $\tilde{v}$ projected on to the nth parabolic cylinder function $D_n(y/y_o)$ and, as shown in Table 1, is related to the nth wave mode with meridional wavenumber n; $\overline{v}$ is the seasonal mean of $\tilde{v}$ and hence the denominator of Eq. (3.1) is the variance of $\tilde{v}$; N is the truncation limit of the series.

Figure 6 shows the error in the fit of the westward- and eastward-moving 200-hPa meridional wind components as a function of y_o for a range of truncations in the series. The 850-hPa results are very similar. For small y_o, the parabolic cylinder functions are strongly equatorially trapped and a large number of terms is required to represent spatial structures in the ±20° equatorial strip. For large y_o, structures away from the equator are well represented, but nearer the equator the errors are larger. In all except the $N = 0$ westward case, there is a minimum total error at intermediate values of y_o. The reduction in error is much smaller with the addition of extra terms beyond $N = 4$. At this truncation the minimum is at $y_o = 6°$, and this is the basic value that will be used in this paper. However, any values for y_o between, say, 5° and 8° could be argued as being relevant.

A range of y_o has been used for reruns of the analysis to be presented in the next section. For any value of y_o
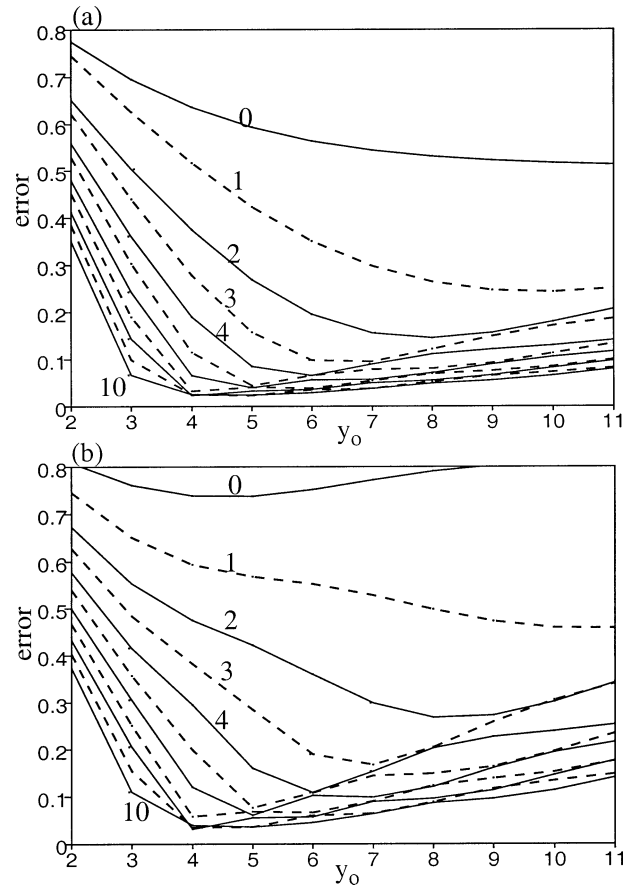

FIG. 6. Space–time mean analysis error in the fit of (a) westward- and (b) eastward-moving 200-hPa meridional wind components as a function of y_o for a range of truncations, $N = 0$–10, in the series defined by Eq (3.1). Numbers indicate the values of N. Solid lines are for N even and dashed lines are for N odd.

in the range 5° to 8°, at each day and level the same physical structures are represented as, for example, $n = 1$ Rossby waves. The smaller the value of y_o, the more equatorially trapped the structures appear. Identifying the structure at consecutive days gives a phase speed from our technique that is, therefore, independent of the particular values of y_o used. This contrasts with the classic equatorial wave theory for which all the wave speeds are derived from $c = 2\beta y_o^2$, and where c is also related to an equivalent depth h by $c = (gh)^{1/2}$. However, it is interesting to use these relations and also to compare with the result given in other studies. The trapping scale $y_o = 6°$ would correspond to $c \approx 20$ m s^{-1} and $h \approx 43$ m. These are also close to the preferred values deduced by Wheeler and Kiladis (1999). Earlier, the work of Kiladias and Wheeler (1995) suggested a rather larger value for y_o, in the range 7° to 14°, for the R1 wave (as determined from their equatorial Rossby radius of deformation of 10°–20°). In contrast, the study of Takayabu (1994a) suggests a value of $y_o = 5°$, at the lower end of the range given here.

4. Identifying structures in the real atmosphere— A case study

This section describes the application of the methodology to a case study of equatorial waves during the 8-day period 12–19 July 1992. Throughout, the values $Y = 20°$, $y_o = 6°$, and $\alpha = g/(2\beta y_o^2)$ will be used, except where stated. To make the computation more tractable, the CLAUS T_b data and ERA dynamical fields have been regridded to a coarser grid of approximately 2.5°. Experiments show that the coarse resolution significantly reduces computing time without affecting the analyzed wave structures.

The complex and rich array of equatorial waves identified during the period is summarized in the third pair of columns in Table 2. The reader may find it useful to refer to this as the waves are identified in the following sections.

a. Westward-moving waves associated with off-equatorial convection at 5°–20°N

As suggested by the summary in Table 2, various convectively coupled WMRG, R1, and R2 waves have been identified at a wide range of locations across the Atlantic, Pacific, and Indian Oceans. The majority of these waves are closely linked to convection, and most of them are present in both the lower and upper troposphere, indicating strong vertical coupling.

As an example of the results, we show the WMRG and R1 waves identified in the upper- and lower-tropospheric winds over the eastern Pacific–Atlantic region during the 8-day period (Fig. 7). These waves have an average zonal wavenumber of about 6, with a longer wavelength over the eastern Pacific region than over the Central American to Atlantic region. They are associated with westward-moving areas of convection, "A" and "B," identifiable in the westward-moving brightness temperature anomalies, which provide the background to each panel in Fig. 7. The WMRG wave is prevalent for the first 4 days (Figs. 7a,b) and the R1 waves dominate for the latter 4 days (Figs. 7c,d).

On 12 July, Fig. 7a shows a maximum upper-troposphere equatorial southward wind over western South America with, from Fig. 7b, a northward wind at low levels. It is clear that these maxima form part of horizontal wind fields that are mainly rotational. The corresponding height fields at both levels show that the circulations are around height field extrema (not shown). The structure therefore looks like a textbook first internal, baroclinic WMRG. Over the next 3 days it retains its structure and moves westward some 8° per day (about 10 m s^{-1}). The brightness temperature clearly contains a variety of components that are symmetric and antisymmetric about the equator. However, the convection in the region of the meridional wind extrema discussed is predominantly antisymmetric. Its spatial relationship, and in particular that of convection region A, with respect to the WMRG is very close to that expected if it is associated with low-level convergence in the wave (cf. Fig. 3). As indicated by the blue line, this relationship is retained over the period shown. We thus consider this to be an example of a convectively coupled WMRG.

The lower troposphere (Fig. 7d) in the region 135°–90°W in the following 4-day period exhibits a westward-moving R1 structure, with the winds being predominantly rotational and circulating around geopotential maxima (not shown). In the upper troposphere (Fig. 7c), a similar structure is indicated. The amplitude is smaller and the sign is the same. With just two levels the details of the vertical structure cannot be determined but in this case it may be barotropic. Such a barotropic vertical structure in the R1 wave was found also over the equatorial central Pacific by Kiladis and Wheeler (1995) and Wheeler et al. (2000). The convection region A has moved further away from, and is more symmetric about, the equator than during the earlier period shown for the WMRG. On 16 July its spatial relationship with the R1 wave is again consistent with the low-level convergence in the wave shown in Fig. 3. Over the next 3 days, the dynamical structure and the convective signature move westward, retaining their integrity. The movement of convection region A is shown by a blue line, which is dashed in the upper troposphere because of the reversed circulation there from that anticipated. Convection region A continues to move further from the equator and, as discussed below, by 19 July is actually associated also with an R2 wave.

Seen also in Figs. 7c and 7d from 17–19 July is a westward-moving R1 structure in the Atlantic, which appears to be coupled with convection region B. This R1 wave has a reversal in circulation through the troposphere suggestive of a first internal baroclinic mode structure.

One of the tests proposed above for the usefulness of the analysis technique is that the separately analyzed u and v fields for the R1 wave, for example, should be predominantly rotational and that these wind components should be approximately in geostrophic balance with the analyzed R1 height field. Quantitative measures of these balances have been obtained, averaged over the tropical strip and over season. By considering these measures as a function of α we can check that the choice made for α on the basis of the geostrophy of the Kelvin wave is more generally applicable. Shown in Fig. 8 are 850-hPa normalized variances of the divergence $\partial u/\partial x + \partial v/\partial y$ and the ageostrophic wind speed $|f\mathbf{v} + g\mathbf{k} \times \nabla\phi|$. In each case the normalization is performed using the variances of the individual terms. At the chosen value of α (1 on the abscissa), there is on average, indeed, a high level of cancellation between the two terms in each case so that the flow is predominantly rotational and geostrophic. It is also clear that the chosen value of α is nearly optimum in this regard.

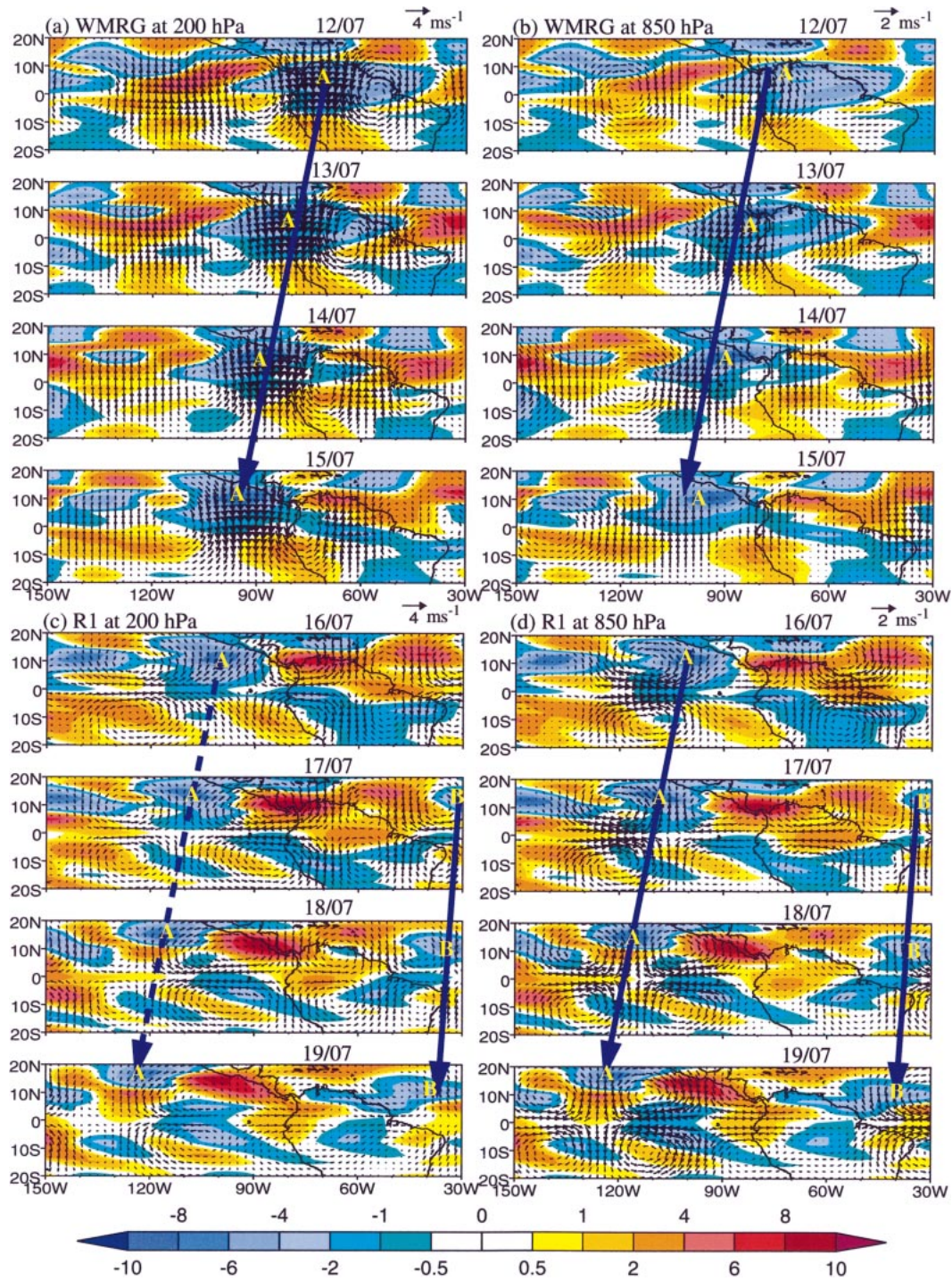Other waves are found during this 8-day period. Accompanying the WMRG and R1 waves shown in Fig.

FIG. 7. Horizontal winds analyzed from the ERA daily data projected onto the $n = 0$ and 1 waves at 30°–150°W, which are identified as the WMRG and R1 waves. The WMRG is for 12–15 Jul 1992 at (a) 200 hPa and (b) 850 hPa; the R1 wave is for 16–19 Jul 1992 at (c) 200 hPa and (d) 850 hPa. Superimposed colors show T_b for the same days. Both data are for westward-moving waves. Characters A and B show convection coupled with the WMRG and R1 waves. Blue arrow line shows the Northern Hemisphere branch of the dynamical wave coherent with convection centers with the first baroclinic structure, and the broken blue line indicates the Northern Hemisphere dynamical branch connected with convection but with a reversed circulation from that of the first internal baroclinic mode. Units are m s^{-1} for wind and K for T_b.
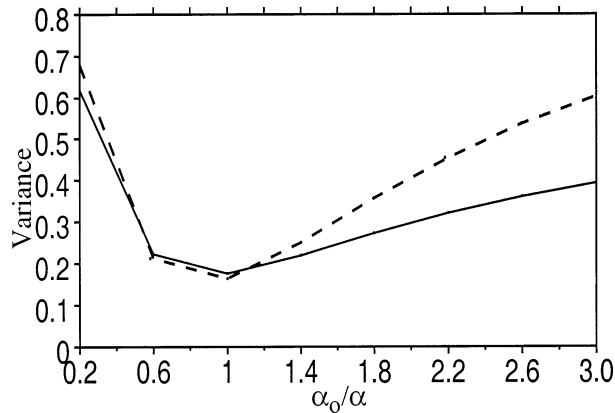
FIG. 8. The 850-hPa normalized variances of the horizontal divergence, $\partial u/\partial x + \partial v/\partial y$ (solid line), and the f times ageostrophic wind speed $|f\mathbf{v} + g\mathbf{k} \times \nabla \phi|$ (dashed line) for the westward-moving $n = 1$ analysis at 850 hPa. This is expected to be dominated by R1 waves but could also include small-amplitude low-frequency WG1 waves. In each case the normalization is performed using the variances of the individual terms. The abscissa shows values of α^{-1} normalized by $\alpha_o = g/(2\beta y_o^2)$, the chosen value used in this analysis.

7, a convectively coupled R2 wave is also found and linked to the convective region A (not shown), although the convection associated with the R2 wave was originally further north of A near 15°–20°N, 30°–100°W, in agreement with the convergence in the dry wave shown in Fig. 3. The coexistence of the $n = 0$ WMRG and $n = 2$ Rossby waves over South America and the eastern Pacific suggests that a linear regression between convection and dynamical fields, even after a separation of symmetric and antisymmetric components and space–time filtering (as done by Wheeler et al. 2000), may still fail to identify/separate dynamical structures of particular waves. This emphasizes the value of our methodology.

The summary given in Table 2 shows that in general the expected waves are present. The suggestion from Doppler shifting, that the WMRG may not be found at low levels in the Eastern Hemisphere is supported during this period. However, Rossby waves are found there. In the upper troposphere in the Western Hemisphere, the WMRG is found. The Rossby wave is also found there but it often has the same sign as at the lower level, suggesting that the ambient flow could indeed be important. A modeling study by Wang and Xie (1996) showed that in a two-level model differing vertical shears can alter the vertical coupling of baroclinic and barotropic components of equatorial waves, significantly affecting the Rossby and WMRG waves, especially the former. Their results suggested that the ratio of the amplitude of the barotropic versus baroclinic modes all increased with increasing strength of the vertical shear, independent of the sign of the shear. Our results for this period do not agree with those of Wang and Xie (1996). The vertical shear in the Western Hemisphere, where the barotropic structure is dominant, is

actually weaker than that in the Eastern Hemisphere where the baroclinic structure is dominant. However, this result is based only on a limited case study and merits further investigation with an extended record to provide more robust statistics, as will be reported on in a later paper.

b. Eastward-moving waves associated with off-equatorial convection at 5°–20°N

A similar analysis has been performed for the eastward-moving components of the T_b and ERA dynamical field data for the same period. The summary of off-equatorial, eastward-moving waves provided in Table 2 indicate that structures related to EMRG, WMRG, R1, R2, and EG waves can all be identified as eastward-moving waves, as hinted at by the Doppler shift argument.

As an example, Fig. 9 shows the eastward-moving T_b and the upper-tropospheric eastward-moving $n = 0, 1$ waves for 13 and 14 July. Since for the same meridional wavenumber n, different wave structures may occur at different longitudes due to variations in the ambient flow, the whole tropical field needs to be shown for these waves. Here we focus on the off-equatorial convection associated with the $n = 0$ and 1 waves, although the convection in Fig. 9 is dominated by the equatorial signature of the Kelvin waves (e.g., regions "C" and "D"), particularly in the Eastern Hemisphere. These Kelvin waves will be discussed in detail in section 4c.

Looking at Fig. 9a in detail, EMRG wave structures, with a zonal wavenumber of 5, appear clearly in the Eastern Hemisphere, between 50° and 120°E, where the flow is easterly and signs of WMRG wave structures with a zonal wavenumber of 6 can been seen between 0° and 90°W, where the ambient flow is westerly (Fig. 4). The appearance of these different types of MRG waves, dependent on the sign of the basic state, is entirely consistent with the suggestions given by the Doppler shift argument. As indicated by the two solid blue lines, these EMRG and WMRG waves are convectively coupled with the two off-equatorial regions of convection, "E" and "F," respectively. Both waves last for more than 3 days. Corresponding structures are not found at 850 hPa.

Figure 9b shows the upper-tropospheric structures of the eastward-moving R1 and EG1 waves (note that the T_b field is the same as in Fig. 9a). The presence of an R1 wave is clearly evident in the Western Hemisphere and a weaker sign of an EG1 wave is seen between 50° and 100°E. Both waves have a wavenumber of about 6. An upper-level R1 wave also appears over the Maritime Continent even though the seasonal mean flow is easterly there. However, during the season there are significant variations in the ambient flow that can also have implications for the presence of different wave structures. During the period 6–14 July, a westerly flow is prevalent in the region 0°–10°S, 100°–150°E, and on 9
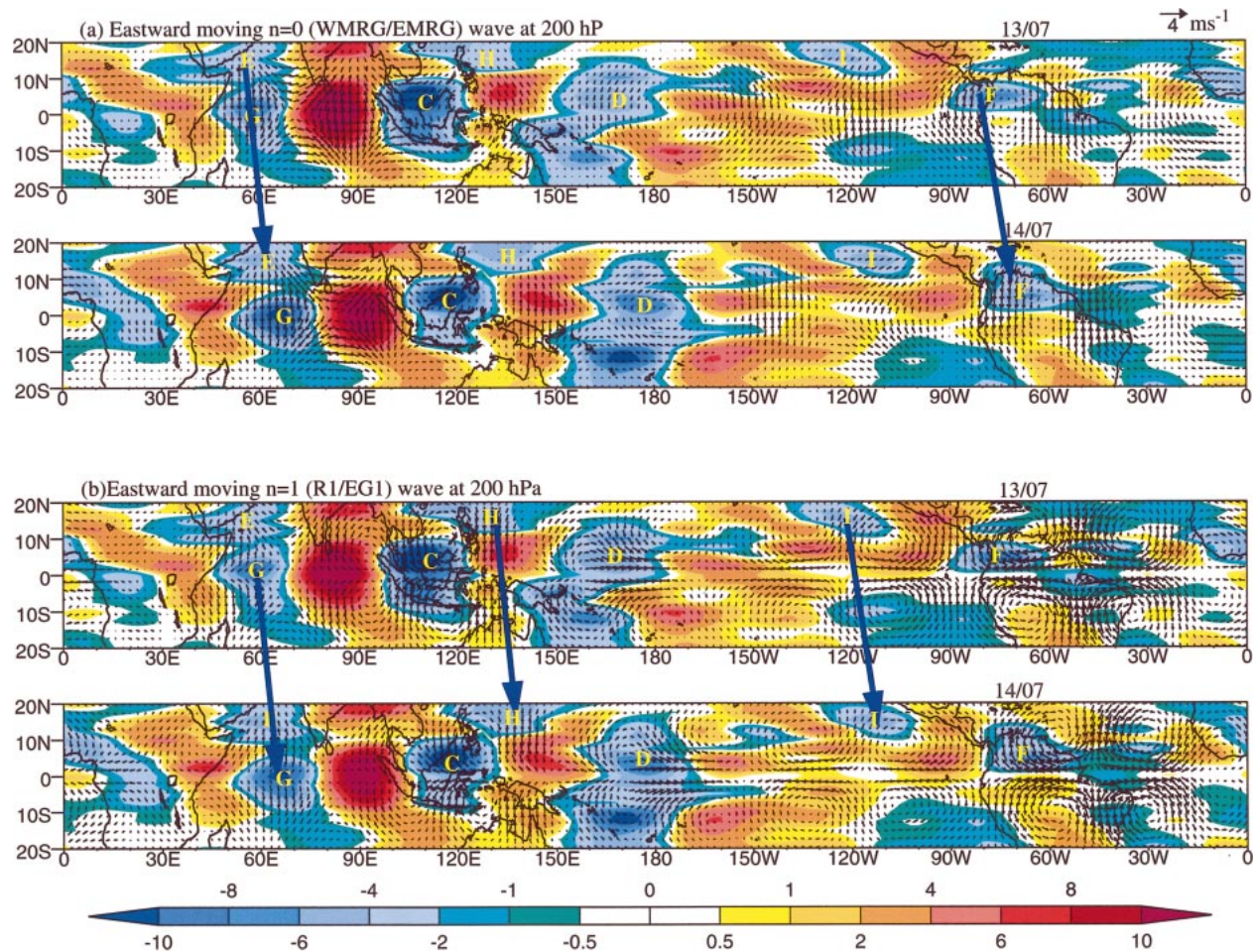
FIG. 9. As in Fig. 7, but for the eastward-moving (a) $n = 0$ and (b) $n = 1$ waves and T_b on 13–14 Jul 1992. Characters E and F show convection coupled with EMRG and WMRG waves, and G, H, and I coupled with the EG1 and R1 waves. Characters C and D are coupled with the Kelvin waves and will be shown in Fig. 10.

July near 120°E, the westerly wind average between 10°N and 10°S is 9 m s^{-1}. These westerlies can therefore support eastward moving R1 waves. Similarly, although Fig. 2 suggests that the dispersion curve for EG1 waves is unlikely to enter the space–time domain of interest, if the ambient flow is sufficiently easterly, say -20 m s^{-1}, then EG waves are possible. Such an ambient flow is not unrealistic. During the period 12–19 July, easterly winds exceeding 20 m s^{-1} do occur in the 50°–80°E equatorial region. These subseasonal variations in the ambient flow therefore allow a mixture of eastward-moving EG1 and R1 waves in the upper troposphere of the Eastern Hemisphere, which again are consistent with the effects of Doppler shifting.

The two blue solid lines around 120°E and 120°W in Fig. 9b indicate coupling of the R1 waves with the areas of convection, "H" and "I." As in the case of the eastward-moving MRG waves, these coupled features also last for more than 3 days. The blue solid line around 60°E indicates the EG1 wave, which is also coupled

with an equatorially centered region of convection, "G," which will be discussed further in section 4c.

In contrast to the upper troposphere, significant eastward-moving R1 waves can only be seen in the lower troposphere of the Eastern Hemisphere. However, these R1 waves are not clearly coupled with off-equatorial convection. Instead they appear to be closely linked with equatorial convection as discussed below in section 4c. The EG1, WMRG, and EMRG waves cannot be clearly seen at the lower level. This difference in the wave behavior between the upper and lower troposphere may be explained by the weaker ambient zonal flow in the lower troposphere (Fig. 4) and the correspondingly smaller impact of Doppler shifting.

Eastward-moving R2 waves in the upper and lower troposphere are identified and are also associated with the convection, E and F. These waves have a first baroclinic structure, but are less coherent in the upper troposphere of the Eastern Hemisphere and the lower troposphere of the Western Hemisphere where, in both

cases, the ambient flow is not favorable for the eastward-moving waves. As for the westward-moving waves described in the previous section, the $n = 0$ MRG and $n = 2$ Rossby waves again coexist and are associated with the same regions of convection.

The three eastward-moving waves coupled with off-equatorial convection (WMRG, R1, and R2) do not appear over the central Pacific region during this period. This may be due to the fact that the westerly winds required for the appearance of such waves are not prevalent in this region, in either the upper or lower troposphere.

The effects of Doppler shifting may inhibit vertical coupling of eastward-moving R1, R2, and MRG waves when the ambient flow in the upper and lower troposphere differs significantly, as is the case for much of the Tropics. As mentioned above and shown in Table 2, compared with the eastward-moving WMRG and R1 waves, the eastward-moving R2 wave is more likely to occur at the both levels and is more vertically coupled. However where the ambient flow is easterly, the wave tends to be less coherent. The reason for the difference between WMRG, R1, and R2 waves is not clear but may be partly that the R2 wave can be Doppler shifted to move eastward in a weaker westerly flow than would be required by the WMRG and R1 waves.

c. Eastward-moving waves coupled with equatorial convection at 5°N–5°S

As shown in Fig. 3, basic theory suggests that equatorial convection linked to low-level convergence is mainly associated with the Kelvin wave. It could also be linked with the other gravest waves, for instance the $n = 1$ gravity wave, but these generally occur on the higher-frequency range.

It is found that, in this period, Kelvin waves dominate in the region 60°E–150°W. Figure 10 gives examples of these waves during 12 to 15 July. Over the Indian Ocean, the region of deep convection C is accompanied by areas of suppressed convection to the west and, to a lesser extent, to the east. These regions of enhanced and suppressed convection move eastward and are mainly symmetric about the equator, with a maximum on the equator. The wind field shown in Fig. 10 confirms that this convection can be associated with an upper-tropospheric Kelvin wave, which has a wavenumber of 6 and moves eastward with a similar phase speed to the convection. Consistently, its convergence and divergence centers coincide, respectively, with the regions of suppressed and enhanced convection, as indicated by the red and blue solid lines.

The lower-tropospheric wind field, shown in Fig. 10b, suggests that the vertical structure of the Kelvin wave is not exactly that of the first baroclinic mode, but has a westward phase tilt with height, consistent with the vertical structure observed in Wheeler et al. (2000). As shown by the red and blue lines linking the region of convection C in Fig. 10b, the lower-tropospheric regions of divergence and convergence are located to the east of the centers of suppressed and enhanced convection. In fact, the enhanced convection is in phase with the lower-tropospheric maximum westerly wind anomaly, as indicated in the red circle of Fig. 3. This is in agreement with the possible importance for convective organization of wind-dependent surface energy fluxes. Assuming that the near surface and 850-hPa zonal winds have similar phases, it does not appear to support the frictional convergence hypothesis. Also the lower-level divergence maximum to the west of convection C moves faster than the convergence to its east and nearly merges into the convergence center at 15 July. This may be responsible for the weakening of the convergence and the associated convection C.

Over the central Pacific, to the east of a region of suppressed convection, there is an area of slightly enhanced convection D, which is closely connected to a lower-tropospheric Kelvin wave. On 12 July, when the convection center is to the north of the equator the lower-level convergence is weak. Subsequently, the convection D moves to the equator, the lower-level convergence intensifies, and the convection and convergence centers move eastward together with a similar phase speed. As the wave moves eastward, the phase shift between the upper and lower troposphere decreases so that by 14–15 July, a convectively coupled Kelvin wave with a first baroclinic structure is clearly seen.

Figures 10a and 10b also show the presence of a region of convection G over the western Indian Ocean. This is not clearly related to a Kelvin wave. As shown in Fig. 9b it is related to the upper-level EG1 wave there. Further analysis indicates that this convection is also closely associated with a lower-level R1 wave (Fig. 10c). As noted in section 4b, Doppler shifting can give rise to lower-tropospheric eastward-moving Rossby waves in the Eastern Hemisphere. An example of this can be seen on 13 and 14 July between 45° and 90°E where the low-level ambient flow is westerly. However, compared with the corresponding theoretical wave structure (Fig. 3), it is clear that this R1 wave is not coupled with off equatorial convection. Instead, it appears to be closely linked with the region of equatorial convection G, which in turn is coincident with the region of enhanced westerly winds in the R1 wave. Noting that the ambient flow at this time is westerly, in excess of 5 m s^{-1}, it seems likely that the wind-induced surface fluxes are again playing an important role in determining the location of the convection associated with the wave. In addition, it is interesting to note that the westerly wind anomalies of the R1 wave, which coincide with the convection, are much stronger than their easterly counterparts suggestive perhaps of feedback between the convection and the dynamics. Furthermore, it could be argued that the convective response to the equatorial zonal winds associated with the R1 wave modifies the
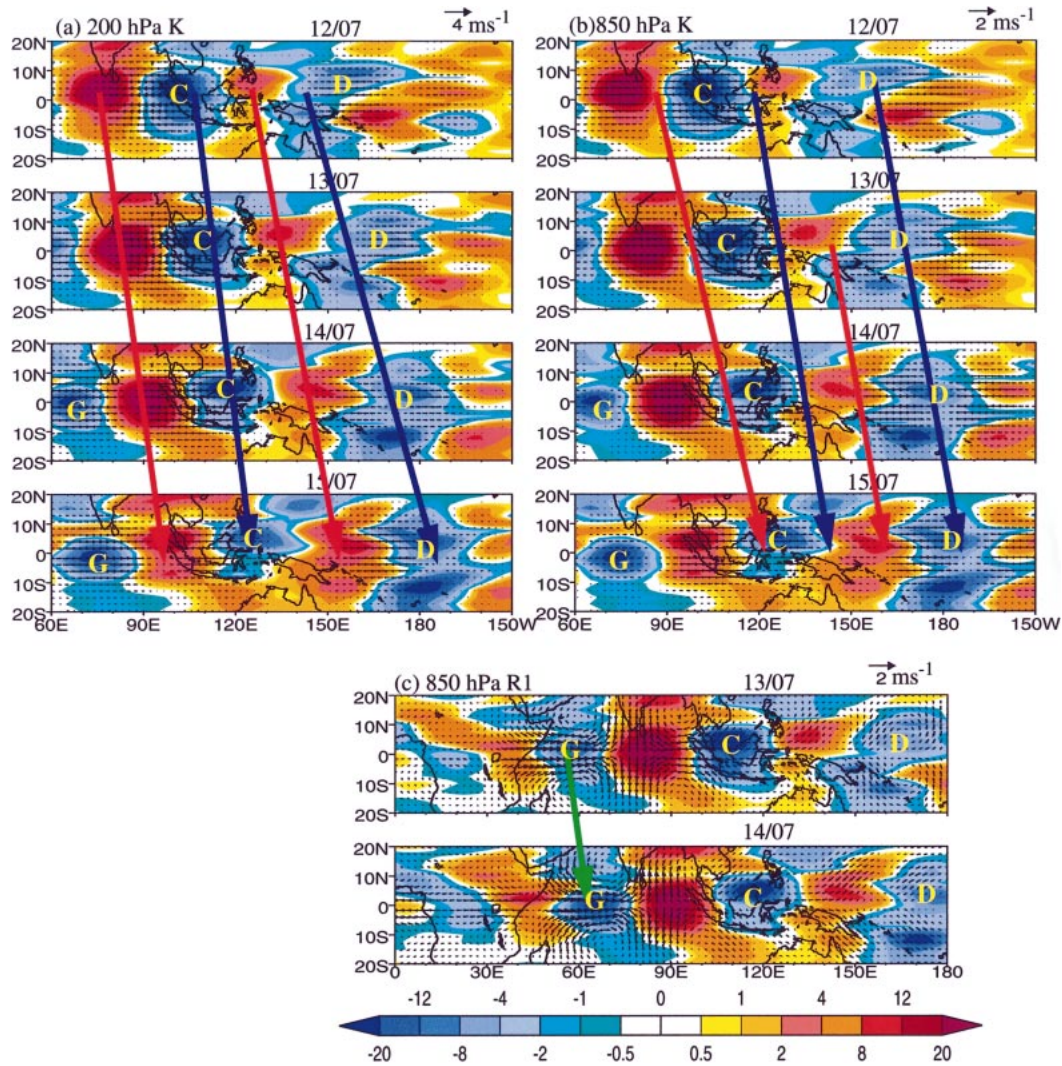
FIG. 10. As in Fig. 7, but for the eastward-moving Kelvin wave and T_b at 60°E–150°W during 12–15 Jul at (a) 200 hPa and (b) 850 hPa, and (c) for an eastward-moving R1 wave at 850 hPa at the Eastern Hemisphere during 13–14 Jul. Characters C and D show convection coupled with the Kelvin wave, and G coupled with the lower level R1 wave. In (a) and (b) the blue (red) arrow lines indicate the upper-level equatorial divergence (convergence) or lower-level convergence (divergence) centers, which are coherent with convection (clear sky). In (c) the green arrow line shows the equatorial maximum westerlies of the R1 wave associated with convection G.

structure of the wave so that it no longer closely resembles its theoretical counterpart.

d. Westward-moving waves coupled with the equatorial convection at 5°N–5°S

The theoretical structures shown in Fig. 3 suggest that only the WG1 wave would connect through its convergence with westward-moving equatorial centered convection. However, unlike EG1, it is not found within the frequency range considered here. Also, as indicated in Table 1, equatorial wave theory suggests that, in contrast to eastward-moving Kelvin waves, there should be no corresponding westward q_o component. However, our analysis of the ERA data in terms of parabolic cyl-

inder functions gave an appreciable westward-moving q_o. Redoing the whole analysis with different values of y_o did not lead to a reduction in this component. It could be reduced by approximately a factor of 1.7 at upper levels and 3.8 at lower levels by decreasing α by a factor of 2.2–3. However, such values are not consistent with either Kelvin wave geostrophy or as can be seen in Fig. 8 comparing the values for $\alpha_o/\alpha = 1$ and $\alpha_o/\alpha = 2.2 - 3$, with the rotational and geostrophic nature of the R1 wave.

It has been found that the appearance of the westward-moving q_o is often accompanied by a lower-tropospheric westward-moving R1 wave, with equatorial convection that is consistent with being induced by the wind-dependent fluxes of the R1 wave. Figure 11 shows an
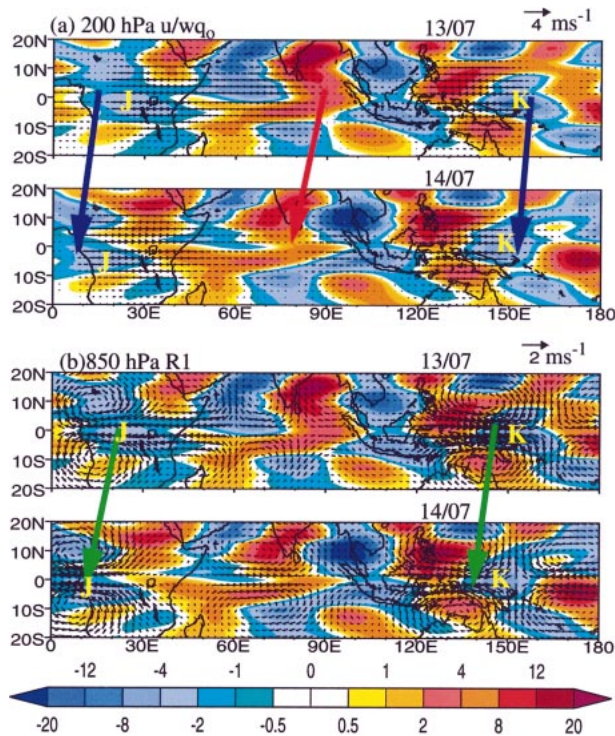
FIG. 11. As in Fig. 7, but for the westward-moving $n = -1$ and 1 waves and T_b on 13–14 Jul 1992 in the Eastern Hemisphere: (a) 200-hPa u associated with $n = -1$ westward q_o (u/wq_o); (b) 850-hPa R1 waves. Characters J and K show convection connected with u/wq_o divergence and u maximum of R1 waves. The blue (red) arrow lines in (a) show the divergence (convergence) of u/wq_o. The green arrow lines in (b) show equatorial maximum easterly and westerly of the R1 wave associated with convection J and K, respectively.

example of the relationship between the upper-tropospheric zonal winds from the westward q_o (labeled u/wq_o) and the lower-tropospheric R1 wave. It is seen that the upper-level u/wq_o is closely associated with equatorial convection, with its divergence connected with regions of enhanced convection, "J" and "K," and convergence over the region of suppressed convection over the eastern Indian Ocean, as indicated by the blue and red solid lines.

As shown by the two green arrow lines in Fig. 11b, the lower-tropospheric R1 wave is closely connected with the same two regions of equatorial convection J and K. These occur in regions of enhanced equatorial zonal flow. For J, this coincides with the region of maximum easterly winds in an easterly ambient flow, whereas for K, it coincides with the maximum westerly winds in a westerly ambient flow during this period. This is again consistent with the hypothesis that wind-induced surface heat fluxes give the association between the R1 wave and equatorial convection.

The method of separating individual wave modes also produces a westward q_o term in the lower troposphere during 17 to 19 July near 90°W. In this case, the convergence of u/wq_o is connected with equatorial convec-

tion and again this event is associated with an R1 wave. Returning to Fig. 7d, we can see that while the R1 wave is coupled with the off-equatorial convection A, it is also connected with a region of equatorial convection to the southeast of A. On 18 and 19 July, when significant easterlies in the lower-tropospheric R1 wave are in phase with the equatorial convection, the convection intensifies. As was the case for the eastern Pacific region, the ambient flow is easterly, suggesting that wind-induced surface fluxes associated with the lower-level R1 wave give rise to an intensification of the equatorial convection and the appearance of a flow described by the u/wq_o term. It is also found, but not shown here, that some cases of activity in u/wq_o may be associated with the convection induced by the enhanced zonal winds of the R2 waves. Although these are off the equator (see Fig. 3), they are sufficiently close to it to significantly modify near-equatorial convection.

5. Conclusions and discussion

In this study, a new methodology has been developed based on shallow water theory that isolates individual equatorial modes in the real atmosphere. It has been used to identify various equatorially trapped waves in observational data. The methodology is different from a space–time spectral filter analysis, which assumes that the linear adiabatic theory for equatorial waves on a resting atmosphere is applicable. Here, it is assumed only that we can use the horizontal structure functions given by equatorial wave theory. The dynamical fields are first separated into eastward- and westward-moving components using space–time spectral analysis and then projected on to different equatorial modes with a best fit trapping scale y_o deduced from the observational data in a suitable latitude belt.

The methodology is applied to the ERA dynamical fields and the CLAUS satellite observed window brightness temperature data. The spatial and temporal consistency of the results suggests that the technique has been successful in identifying equatorial wave structures and in detecting some important characteristics of equatorial modes. A best fit trapping scale $y_o = 6°$ for tropical latitudes 20°N–20°S has been deduced. By comparing the eastward- and westward-moving components of the convection field, inferred from the satellite T_b data, we have been able to detect convectively coupled equatorial waves.

The general consistency of the spatial and temporal structure of the individual wave components identified in the 8-day period and of the convection with them has given confidence that the methodology has been successful. As summarized in Table 2, we have found evidence of off-equatorial convection limited not only to the expected westward-moving WMRG and Rn waves. Consistent with some validity of the notion of Doppler shifting by the ambient wind, at the upper level we have also found eastward-moving EMRG, Rn, and EG1

waves in the Eastern Hemisphere, and WMRG and Rn waves in the Western Hemisphere. Near-equatorial convection has been found to be associated not just with eastward-moving Kelvin waves but also with the zonal wind in modified Rossby waves moving in both directions. Most of the waves show first internal mode behavior or amplitude concentrated at one level. However, R1 waves in the eastern Pacific and eastern Atlantic regions have the same sign in the upper and lower troposphere, evidence of barotropic or mode-2 behavior.

All the waves mentioned above, apart from the R1 wave, appear to have convection associated with their low-level convergence or, in the case of the Kelvin wave, possibly with a low-level zonal wind maximum. It appears that such convection does not radically change the dry wave structure, though the Kelvin wave has a tilt in the vertical. However, it appears that equatorial or near equatorial convection can be associated with the low-level zonal wind extrema in these waves, consistent with it being associated with a maximum in surface energy fluxes. The westward-moving q_o, which is found in the data but not given by dry theory, appears to be associated with the Rossby wave. Therefore, the hypothesis is made that Rossby waves coupled with equatorial convection can exist and have a new structure involving a westward-moving q_o, as well as the dry wave components. The different vertical structure of some of the Rossby waves may also be evidence of a changed structure due to the convective coupling. Further investigation into those aspects is required with a more extensive set of data. This is the aim of a companion paper on this study.

It is hoped that the analysis method will make a very powerful diagnostic method for investigating convectively coupled equatorial waves and the interaction of equatorial dynamics and physics in the atmosphere. Comparison of the results of applying similar analyses to climate and weather forecast models should give considerable insights into their behavior. A parallel diagnosis of the ECMWF 40-Year Reanalysis (ERA-40) data and model validation will also be performed in a subsequent study. Key questions will be addressed concerning the interaction between dynamics and convection, and how well this is represented in models.

REFERENCES

Dunkerton, T. J., and M. P. Baldwin, 1995: Observation of 3–6-day meridional wind oscillations over the tropical Pacific, 1973–1992: Horizontal structure and propagation. *J. Atmos. Sci.,* **52,** 1585–1601.

Emanuel, K. A., 1987: An air–sea interaction model of intraseasonal oscillation in the Tropics. *J. Atmos. Sci.,* **44,** 2324–2340.

Gill, A. E., 1980: Some simple solutions for heat induced tropical circulations. *Quart. J. Roy. Meteor. Soc.,* **106,** 447–462.

——, 1982: *Atmosphere–Ocean Dynamics.* Academic Press, 662 pp.

Gruber, A., 1974: The wavenumber-frequency spectra of satellite-measured brightness in the Tropics. *J. Atmos. Sci.,* **31,** 1675–1680.

Hayashi, Y., 1982: Space–time spectral analysis and its applications to atmospheric waves. *J. Meteor. Soc. Japan,* **60,** 156–171.

Hendon, H. H., and B. Liebmann, 1991: The structure and annual variation of antisymmetric fluctuations of tropical convection and their association with Rossby–gravity waves. *J. Atmos. Sci.,* **48,** 2127–2140.

——, and M. L. Salby, 1994: The life cycle of the Madden–Julian oscillation. *J. Atmos. Sci.,* **51,** 2225–2237.

Hodges, K. I., D. W. Chappell, G. J. Robison, and G.-Y. Yang, 2000: An improved algorithm for generating global window brightness temperatures from multiple satellite infrared imagery. *J. Atmos. Oceanic Technol.,* **17,** 1296–1313.

Hoskins, B. J., and G.-Y. Yang, 2000: The equatorial response to higher-latitude forcing. *J. Atmos. Sci.,* **57,** 1197–1213.

Kiladis, G. N., and M. Wheeler, 1995: Horizontal and vertical structure of observed tropospheric equatorial Rossby waves. *J. Geophys. Res.,* **100,** 22 981–22 997.

Lau, K.-M., 1981: Oscillation in a simple equatorial climate system. *J. Atmos. Sci.,* **38,** 248–261.

——, and L. Peng, 1987: Origin of low frequency (intraseasonal) oscillations in the tropical atmosphere. Part I: Basic theory. *J. Atmos. Sci.,* **44,** 950–972.

Lim, H., and C.-P. Chang, 1983: Dynamics of teleconnections and Walker circulations forced by equatorial heating. *J. Atmos. Sci.,* **40,** 1897–1915.

Lindzen, R. S., and J. R. Holton, 1968: A theory of the quasi-biennial oscillation. *J. Atmos. Sci.,* **25,** 1095–1107.

Madden, R. A., and P. R. Julian, 1972: Description of global-scale circulation cells in the tropics with a 40–50 day period. *J. Atmos. Sci.,* **29,** 1109–1123.

Magaña, V., and M. Yanai, 1995: Mixed Rossby–gravity waves triggered by lateral forcing. *J. Atmos. Sci.,* **52,** 1473–1486.

Matsuno, T., 1966: Quasi-geostrophic motions in the equatorial area. *J. Meteor. Soc. Japan,* **44,** 25–43.

Moscowitz, B. M., and C. S. Bretherton, 2000: An analysis of frictional feedback on a moist equatorial Kelvin mode. *J. Atmos. Sci.,* **57,** 2188–2207.

Neelin, J. D., I. M. Held, and K. H. Cook, 1987: Evaporation-wind feedback and low-frequency variability in the tropical atmosphere. *J. Atmos. Sci.,* **44,** 2341–2348.

Redelsperger, J.-L., and Coauthors, 1998: Review of convection in TOGA-COARE. *Proc. CLIVAR/GEWEX COARE98 Conf.,* Boulder, CO, WCRP, 16–42.

Takayabu, Y. N., 1994a: Large scale cloud disturbances associated with equatorial waves. Part I: Spectral features of the cloud disturbances. *J. Meteor. Soc. Japan,* **72,** 433–449.

——, 1994b: Large scale cloud disturbances associated with equatorial waves. Part II: Westward propagation of inertio-gravity waves. *J. Meteor. Soc. Japan,* **72,** 451–465.

Wang, B., 1988: Dynamics of tropical low-frequency waves: An analysis of the moist Kelvin wave. *J. Atmos. Sci.,* **45,** 2051–2065.

——, and X. Xie, 1996: Low-frequency equatorial waves in vertically sheared zonal flow. Part I: Stable waves. *J. Atmos. Sci.,* **53,** 449–467.

Wheeler, M., and G. N. Kiladis, 1999: Convectively-coupled equatorial waves: Analysis of clouds and temperature in the wavenumber–frequency domain. *J. Atmos. Sci.,* **56,** 374–399.

——, ——, and P. Webster, 2000: Large-scale dynamical fields associated with convectively coupled equatorial waves. *J. Atmos. Sci.,* **57,** 613–640.

Yang, G.-Y., and J. Slingo, 2001: The diurnal cycle in the Tropics. *Mon. Wea. Rev.,* **129,** 748–801.

Zangvil, A., 1975: Temporal and spatial behavior of large-scale dis-

turbances in tropical cloudiness deduced from satellite brightness data. *Mon. Wea. Rev.,* **103,** 904–920.

——, and M. Yanai, 1981: Upper tropospheric waves in the Tropics. Part II: Association with clouds in the wavenumber-frequency domain. *J. Atmos. Sci.,* **38,** 939–953.

Zhang, C., 1996: Atmospheric intraseasonal variability at the surface in the tropical western Pacific Ocean. *J. Atmos. Sci.,* **53,** 739–758.

——, and M. J. McPhaden, 2000: Intraseasonal surface cooling in the equatorial western Pacific. *J. Climate,* **13,** 2261–2276.